論文

Assessment of Plastic Constraint Effects Induced by Whisker Interactions in Whisker Reinforced Metal Matrix Composites

Hong Gun Kim*

휘스커 강화 금속기지 복합재료에서의 휘스커 상호작용에 의해 발생되는 소성구속 효과에 대한 평가

김 홍 건*

초 록

본 연구의 목적은 휘스커로 보강된 금속기지 복합재료의 강화 메카니즘이 휘스커간의 상호작용으로 인한 소성구속 효과에 기인한다는 것을 보이는 것이며 이를 위하여 정렬된 단일 휘스커 모델에 대한 두가지의 경우, 즉 소성구속 및 비구속 조건하에서의 거동을 조사하였다. 해석방법으로는 소성증분 이론에 근거한 축대칭 유한요소 모델을 적용하였으며 탄소성 변형상태에서의 소성구속 효과를 평가하기 위하여 영역별 평균값에 근거한 응력분류기법을 착안하였다. 이에 대한 해석결과, 소성구속 및 비구속 조건 각각에서의 영역별 응력-변형률 선도, 기지재의 소성역 전개과정 및 휘스커 내부 응력분포 등을 비교 평가함으로써 소성구속 효과가 복합강화 메카니즘에 지대한 영향을 미친다는 것을 정량적으로 입증하였다. 또 이 효과로 인한 기지재에서의 영역별 정수응력을 계산하여 휘스커단의 기지재에 3축성이 발생된다는 것을 보임으로써 이와 관련된 휘스커의 하중 지지능력 및 파괴 메카니즘도 검토하였다.

ABSTRACT

The purpose of this study is to show that the strengthening mechanism of whisker reinfored metal matrix composites results from the formation of constraint condition induced by whisker/whisker interactions. An aligned axisymmetric single whisker model for the constraint and unconstraint condition has been analyzed to assess the field quantities as well as macroscopic constitutive responses. A domain-based stress grouping approach has been developed to study the plastic constraint effects. Hydrostatic stresses resulting from the triaxiality in the matrix between whisker ends were quantitatively evaluated implementing above approaches. It has been found that whisker stresses are very sensitive to the constraint effects and thus give an enhanced load bearing capability. Finally, the implication of fracture micromechanisms has been discussed in the standpoint of a domain-based constitutive response.

1. INTRODUCTION

Current interest in the metal matrix composites (MMCs) containing discontinuous reinforcements of SiC particles or whiskers stems from their markedly higher stiffness and strength to weight ratio, their quasi-isotropic properties, and their relative ease of fabricability[1~3]. A significant

* 전주대학교 기계공학과

amount of research has been performed to understand the strengthening mechanisms of these materials, but a consensus has not yet been reached. One of the major strengthening mechanisms proposed before is the matrix strengthening due to the enhanced dislocation density caused by a difference in the coefficient of thermal expansion (CTE) between components[4~10]. It presumes that the difference of dislocation density be reflected in an increase in microhardness values for the reinforced matrix material. However, this was not observed experimentally for the Al 2124 with SiC whisker composite system where the range of microhardness values for the composite matrix is roughly the same as that of the control alloy [11].

The other strengthening mechanism proposed is the strengthening arising from the constrained plastic flow and clustering in ductile matrix due to the presence of brittle reinforcements [11]. In the flow regime of shear deformable metallic matrix, the plastic constraint effects for a sufficient number of closely spaced brittle phase should be produced due to the cell boundary compatibility. However, only limited analytical treatments have been studied on the effects of constraint plastic flow in the ductile matrix of the composite due to the presence of the brittle phase. Furthermore, it has been analyzed only for the role of matrix [11, 12].

In this paper, it was focused on the investigation of the detailed composite strengthening mechanism and the related local deformation evolution as well as the macroscopic constitutive response. An axisymmetric finite element analysis (FEA) based on incremental plasticity theory using *von* Mises yield criterion and Plandtl-Reuss equation was implemented to evaluate both the constrained representative volume element (RVE) and the unconstrained RVE. Results were presented of the domain-based decomposed whisker and matrix stresses in MMCs. Further, the role of whisker and matrix on composite strengthening due to plastic constraint effects was rigorously evaluated. The load bearing capability of a whisker and fracture micromechanisms were also emphasized and discussed in detail.

2. FINITE ELEMENT MODELING APPROACH

The approach in this work is centered on the elastoplastic FEA with small strain plasticity theory [13] using an axisymmetric single whisker model as shown in the previous work [14]. In this study, an axisymmetric FE model based on incremental plasticity theory using *von* Mises yield criterion, Plandtl-Reuss equations and isotropic hardening rule. The strains here are assumed to develop instantaneously. For material nonlinearity, the computational difficulty is that the equilibrium equations should be written using material properties that depend on strains, but strains are not known in advance. To solve nonlinearity, Newton-Raphson method has been implemented here. Consistent with small strain theory,

$$\{d\varepsilon^{el}\} = \{d\varepsilon\} - \{d\varepsilon^{pl}\} \quad \cdots\cdots\cdots\cdots (1)$$

where $\{d\varepsilon\}$, $\{d\varepsilon^{el}\}$ and $\{d\varepsilon^{pl}\}$ are changes in total, elastic, and plastic strain vectors, respectively. Elastoplastic stress-strain matrix can be solved iteratively, in which the elastic strain vector is updated at each iteration and the element tangent matrix is also updated. The preset criterion for convergence, i.e. plasticity ratio, was used as 1% at all integration points in the model. According to *von* Mises theory, yielding begins under any states of stress when the effective stress σ_e exceeds a certain limit, where

$$\sigma_e = \left[\frac{1}{2}\{(\sigma_x-\sigma_y)^2+(\sigma_y-\sigma_z)^2+(\sigma_x-\sigma_z)^2\right.$$

$$+ (\tau_{xy}^2 + \tau_{yz}^2 + \tau_{xz}^2)\}\Big]^{1/2} \quad \cdots\cdots\cdots\cdots (2)$$

Detailed procedures to solve material plasticity is described in reference [13]. In FEA modeling, a uniform whisker distribution with an end gap value equal to transverse spacing between whiskers was selected. The whiskers were assumed as uniaxially aligned with no whisker/matrix debonding allowed for, in keeping with the actual situation in many MMCs [15]. The two dimensional view of aligned whisker model is shown in Fig. 1.

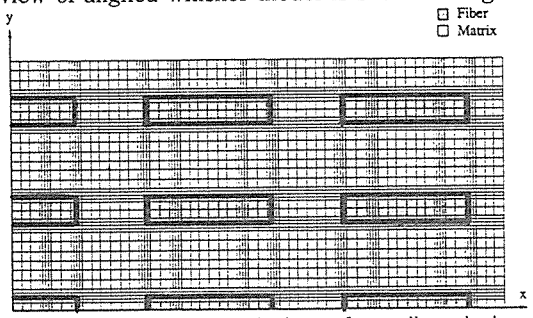

Fig. 1. Two dimensional view of an aligned short fiber or whisker reinforced composite.

From this regular whisker arrangement, a hexagonal cross section can be delineated with whisker/whisker interaction effects as shown in Fig. 2(a). The schematic of axisymmetric RVE is shown in Fig. 2(b). Using this RVE, the FE meshes with symmetric and loading boundary conditions were generated as shown in Fig. 2(c). The FE computations were performed using for noded isoparametric elements [13]. The constrained boundary condition enforces elastic and plastic constraint by requiring that the radial and axial boundary of RVE is maintained in the straight manner during deformation as imposed in the previous work [14, 16].

With Respect to whisker alignment, Takao *et al.* [17] concluded that a misorientation angle of less than 10° has little effect on the composite stiffness, while a misorientation angle greater than 15°~20° has a great effect. Quantitative measu-

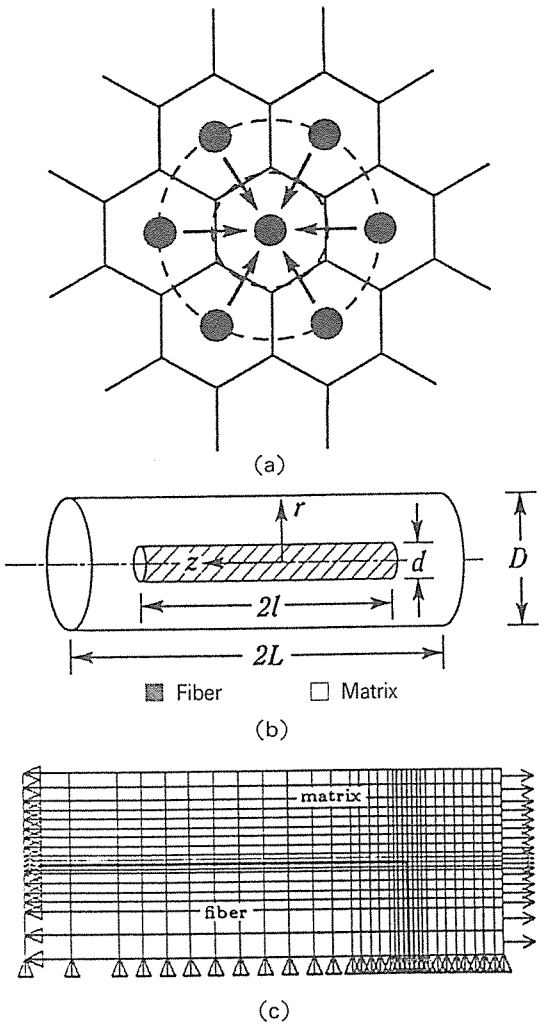

Fig. 2. (a) Cross section of a hexagonally packed MMC with whisker/whisker interactions, (b) Representative volume element(RVE) of a short fiber or whisker reinforced composite, (c) Finite element meshes with symmetric and loading boundary conditions.

rements of the whisker misorientation of this material were not made, but visual observations confirmed that the extrusion process has caused a high degree of whisker alignment. In the previous work [18], the predictions of composite properties using FE models were compared to experimental measurements, and it was concluded

that the effects of whisker misorientation were not of first order significance for the samples.

On the other hand, we can implement the concept of volume average method. The overall stress in a domain can be calculated through a simple averaging scheme given by the following equation:

$$\langle \sigma_{ij} \rangle_{\Omega} = \frac{\int_{\Omega} (\sigma_{ij})_k \, V_k \, d\Omega}{\int_{\Omega} V_k \, d\Omega} \qquad \cdots\cdots\cdots\cdots (3)$$

where $(\sigma_{ij})_k$ is the stress in element k and V_k is the volume of that element. Hence, equation (3) can be used to group each domain stress. Hence, the average stress-strain response is obtained in each domain, which represents regional RVE stresses. By employing this stress grouping approach, a representative domain-based stress-strain curve can be delineated. In a short fiber or whisker reinforced MMC, the composite domain Ω_c can be decomposed into the whisker region Ω_w and the matrix region Ω_m as shown in Fig. 3, and in the same fashion, the field quantity in the matrix region Ω_m can also be decomposed to the surrounding matrix region Ω_{m1} and the matrix region between whisker ends Ω_{m2} as shown in Fig. 4. This stress grouping is, actually, based on the additionally generated stress components under uniaxial loading with constrained condition, of which rationale is explained as follows.

In the unconstrained model, which has a traction free side wall, the whisker end region is more deformed radially and tangentially than that of the constrained side wall. In the domains of Ω_w, Ω_{m1} and Ω_{m2}, presumably, additional stresses are produced due to constraint effects. In domains of Ω_w and Ω_{m1}, compressive radial and hoop stresses are generated. In constrast, additional tensile radial and hoop stresses in Ω_{m2} are produced. Note that, the domain boundaries of Ω_{m1} and Ω_{m2} were grouped as a straight manner for convenience. Thus far, the stress grouping approach was intended to analyze the domains of Ω_w, Ω_m, Ω_{m1} and Ω_{m2} so as to compare the field quantities of constraint case to those of unconstraint case.

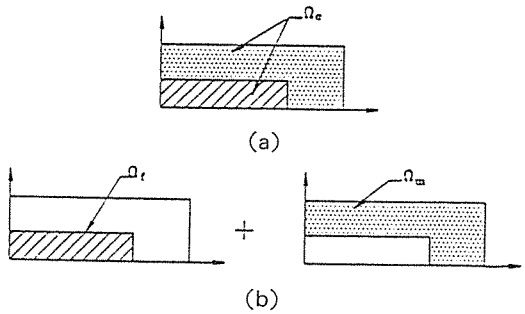

Fig. 3. Schematic of the stress grouping technique in a short fiber or whisker reinforced composite. (a) composite domain, (b) decomposed fiber and matrix domains.

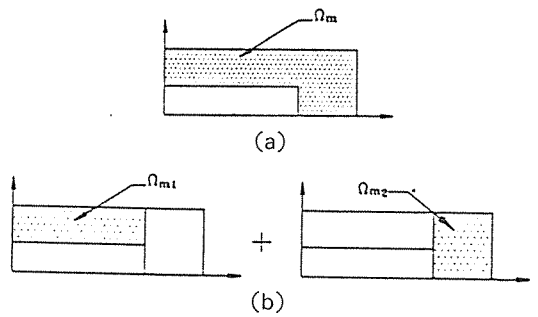

Fig. 4. Schematic of the stress grouping technique in the matrix. (a) overall matrix domain, (b) decomposed matrix domains.

3. EXPERIMENTAL AND MATERIAL PROPERTIES

Both composite and control alloy for the experiment were obtained from the ARCO chemical company. The compacted billets were machined for the cylindrical tension and compression samples with a reduced gage section 0.25 inch in diameter and 4.4 inch long. These samples were then solution heat treated in Argon and drop quenched directly into water. Then, aging was performed in the temperature-controlled bath.

Tensil stress-strain curves for the Al 2124 co-

ntrol alloy and the Al 2124 composite reinforced by 20 vol.% SiC whisker were obtained using strain controlled test at a strain rate of 10^{-3}/sec using Instron 1330 Servo-hydraulic test machine at room temperature. The unreinforced Al 2124 was processed in an identical fashion to the composite, namely, by a powder metallurgy (PM) process involving hot processing above the solidus followed by hot extrusion. The SiC whiskers are approximately 1 μm in diameter with an average aspect ratio of 4 and tend to be aligned in the extrusion direction which corresponds to the longitudinal axis of the tensile samples. After machining, the samples were heat treated for T-6 condition. All tensile tests were performed in accordance with the ASTM standard test method, *Tension testing of metallic materials* (ASTM E-8). From the matrix test data, a multi-linear representation of the matrix stress-strain curve was used for input data. Thus, the stress-strain characteristics of the matrix were defined by the elastic (Young's) modulus, yield stress, and work hardening rate (tangent modulus). These characteristics were measured at room temperature on the PM 2124 Al alloy and were found to be E_m=70 *GPa*, σ_{my}=336 *MPa*, and E_T=1.04 *GPa*, respectively. Other material properties selected were ν_m=0.33 for matrix and E_w=480 *GPa*, ν_w=0.17 for reinforcement [19]. Here, E is Young's modulus, E_T is tangent modulus, σ_{my} is matrix yield stress and ν is Poisson's ratio. The whisker and matrix materials were assumed to be isotropic and the elastic constants were assumed to be temperature independent.

4. RESULTS AND DISCUSSION

The constitutive response of MMCs is strongly affected by the boundary conditions of RVE [16]. Numerical results on the side wall constraint and unconstraint conditions were compared for the macroscopic composite stress-strain responses with the experimental data and for the evolution of plasticity during far field tensile loading. To obtain the monotonic stress-strain relation, the applied far field tensile strain ε_c was started from 0% to 1% and 25 small load steps of which step has maximum 20 iterations were performed incrementally by $\Delta\varepsilon_c$=0.04%. Fig. 5 illustrates the dependency of the overall constitutive responses. While the FEA prediction for deformation "with constraint" overestimates the flow stress of the composite, the calculated flow stress for deformation "without constraint" underestimates because of the lack of whisker/whisker interactions. However, the tendency of numerically predicted composite behavior in the extensive flow regime is obviously shown that the difference between unconstraint results and the experimental data becomes larger than that of the constraint results. Owing to whisker/whisker interactions, additional stresses are produced. The additional matrix stress com-

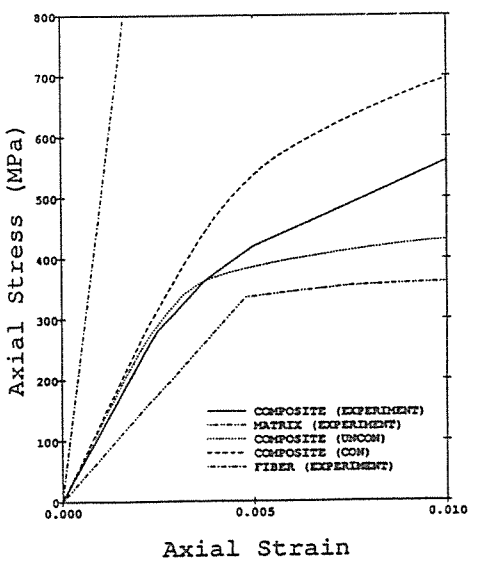

Fig. 5. Stress-strain curves of the experimental results with FEA predictions from the RVE with and without constraint conditions for a peak aged matrix condition of Al 2124 / 20% SiC whisker composite.

ponent which has the pronounced effects on composite strengthening has been shown as the compressive radial stress of the matrix sandwiched by whiskers. It accelerates plastic yielding whereas the tensile radial stress of the matrix between whisker ends suppresses the evolution of plasticity [16]. The difference between results calculated with constraint condition and measured tensile properties is considered from the deviations in the structure of composite by the idealization of equally spaced cylindrical whiskers of identical size, interfacial damage free deformation by perfect bonding assumption and perfectly aligned assumption.

Fig. 6 shows the comparison of local plastic deformation from ε_c=0.16% through ε_c=0.68% incrementally ($\Delta\varepsilon_c$=0.04%). For both constraint and unconstraint cases, the local plastic deformation is initiated in the vicinity of the whisker tip region and developed in the matrix region between whisker ends due to the high stress concentrations. This early plasticity near whisker tip supports the fracture micromechanism proposed by Nutt and Coworkers [20,21]. As can be seen in Fig. 6, the plasticity of the matrix in unconstrained model shows a "confined plasticity evolution" which can not enhance the whisker stresses due to sectional equilibrium for axial stress component. On the contrary, the matrix of const rained model gives a gradual evolution of plasticity so that the whisker stresses are enhanced substantially.

Fig. 7 and 8 show the decomposed stress-strain

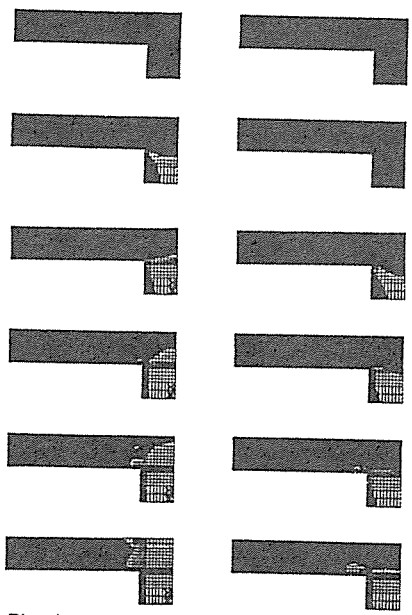

Fig. 6. Plastic deformation evolution in the matrix with and without constraint conditions. The far-field strains are ε_c=0.16, 0.20, 0.24, 0.28, 0.32, 0.36, 0.40, 0.44, 0.48, 0.52, 0.56, 0.60, 0.64, 0.68% from the top to the bottom. All figures of left column are without constraint condition and those of right column are with constraint condition. Black and white regions represent elastic and plastic deformations, respectively.

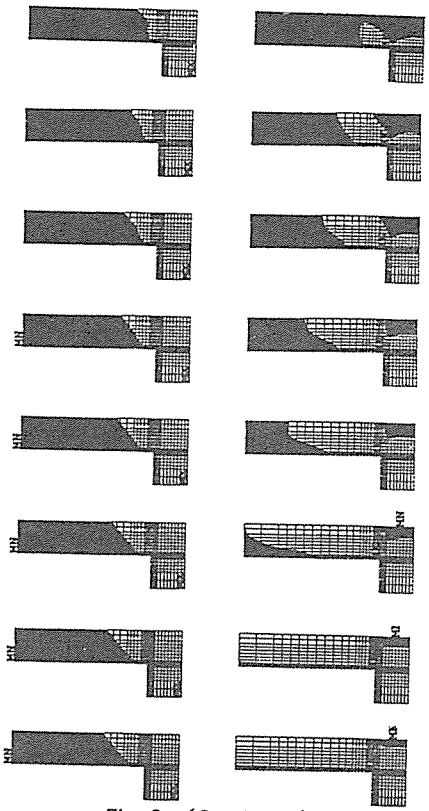

Fig. 6. (Continued)

relations using stress grouping approach. In the domain Ω_m, it was found that the behaviors of both constrained and unconstrained models are not much deviated from the control alloy though flow stresses of unconstrained matrix is a little less than

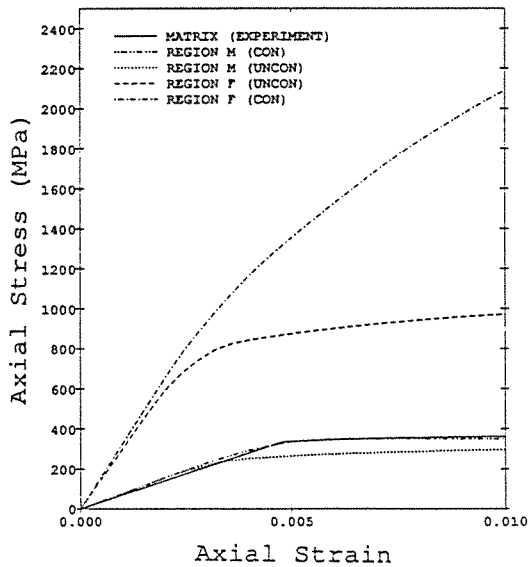

Fig. 7. Stress-strain curves for the whisker and matrix with and without constraint conditions.

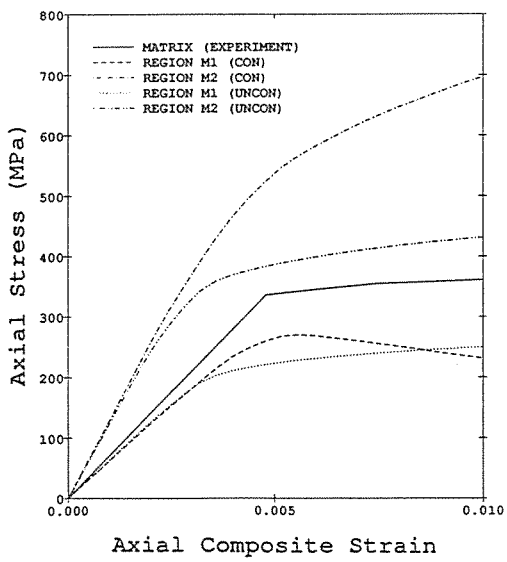

Fig. 8. Stress-strain curves for the decomposed matrix and without constraint conditions.

those of constrained matrix as shown in Fig. 7. However, the whisker stresses between two models show a fundamental difference. This result explicitly indicates that the major composite strengthening mechanism comes from the role of whisker. For the constrained model shown in Fig. 8, the axial flow stress in the region of Ω_m sandwiched by whiskers decreases as the far-field load increases after general matrix yielding whereas that of Ω_m between whisker ends increases. As a result, the total matrix flow stress shows a little difference from the control alloy.

Hydrostatic stresses in Ω_m, Ω_{m1} and Ω_{m2} for the constrained and unconstrained model are shown in Fig. 9. The pronounced constraint effects on hydrostatic stresses also stem from the domain Ω_{m2} as shown in the figure. Hydrostatic stresses in the domain Ω_{m2} show markedly high values because of the additionally generated tensile triaxiality for the constrained model. This enhancement of hydrostatic stresses results in the expa-

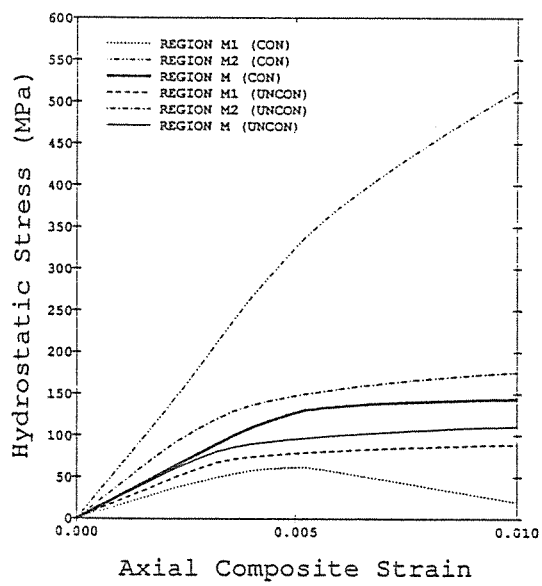

Fig. 9. Hydrostatic stress-strain curves for the decomposed matrix with and without constraint conditions.

nsion of yield surface, which prohibits an extensive plastic deformation. Nevertheless, hydrostatic stresses in domain Ω_{ml} for the constrained model decrease as the far field load increases due to the additionally generated compressive radial stress component. Thus far, the resulting matrix hydrostatic stress for the constrained model shows slightly higher values than that of the unconstrained model.

More detailed whisker stresses including the matrix region between whisker ends are shown in Fig. 10. The axial stresses along the whisker center line are described with the comparison of unconstrained results. The distance from the whisker center was normalized with whisker radius r. The unconstrained model shows a "nearly saturated stresses" when the applied stress reaches about the matrix yield stress, which means that whisker stresses no longer develop to a large extent as the far-field stress increases. It is clearly related to the "confined evolution" of plasticity (*see* left column of Fig. 6). On the contrary, the whisker axial stresses of constrained model develop substantially, which is related to the plastic deformation shown in the right column of Fig. 5. Obviously, the sectional equilibrium enhances axial component stresses significantly by producing triaxiality in the matrix flow regime. Fig. 10 shows that the maximum whisker stress is fairly proportional to the macroscopic composite strain. It can be well over 2 *GPa* at 1% far-field strain. The implication of this result indicates that the major composite strengthening mechanism stems from the whisker strengthening generated by sectional equilibrium in the axial direction based on tensile triaxiality in the matrix. The high whisker stress intensification is important from the standpoint of potential whisker fracture during the deformation of MMCs. Preliminary results [22] suggest that whiskers actually fracture during tensile straining.

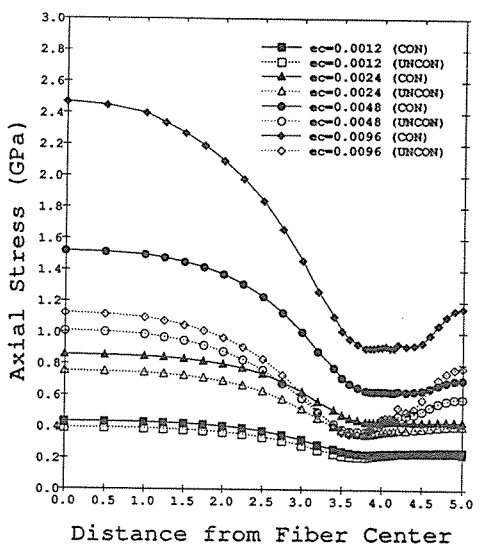

Fig. 10. Whisker stresses on the center line as a function of normalized distance by whisker radius with and without constraints.

On the other hand, the failure mechanism proposed by Nutt and Duva [20], Nutt and Needleman [21], and Needleman [23] involves the nucleation of voids in whisker tip regions due to the stress concentration resulting in lower ductility. The whisker pull-out with coated matrix due to strong interface has also been reported [15], which supports that the failure mechanism stems from the void initiation and coalescence based on dimpled fracture surface. However, the results of present study give a potential that the whisker fracture can be a controlling mode as shown in the previous experiment[22]. Presumably, the failure mechanism of whisker fracture must be more rigorous when composites are made ideally with perfect whisker arrangement, low scattering of whisker aspect ratio, perfect bonding forces, etc. Likewise, the whisker fracture mode will be deviated when the deformation involves highly scattered whisker aspect ratio, clustering, damage induced failure, and/or any other nonidealized

factors.

5. CONCLUSIONS

A continuum analysis of the monotonic tensile stress-strain behavior for constraint effects as well as localized quanitities based on a full numerical solution for an aligned RVE in MMCs has been evaluated rigorously. In all cases, it was found that the constraint boundary condition plays an important role in the macroscopic constitutive response as well as the microscopic plastic deformation evolution. A domain-based stress grouping technique was developed and the results showed that the whisker can contribute significantly to the composite strengthening caused by the formation of matrix triaxiality resulting from constraint effects.

REFERENCES

1. Divecha, A.P., Fishman, S.G., and Karmarkear, S.D., "Silicon Carbide Reinforced Alumunum - A Formable Composite," *Journal of Metals*, 1981, pp.12-17.

2. Nair, S.V., Tien, J.K., and Bates, R.C., "SiC Reinforced Aluminum Metal Matrix Composites," International Metals Review, Vol.30, No.6, 1985, pp.275-290.

3. Kelly, A. and MacMillan, N.H., "*Strong Solid*", 3rd Ed., Clarendon Press, Oxford, 1986, p.240.

4. Arsenault, R.J. and Fisher, R.M., "Microstructure of Fiber and Particulate SiC in 6061 Al Composites," *Scripta Metallurgica*, Vol.7, 1983, pp.67-71.

5. Arsenault, R.J. and Taya, M., "The Effects of Difference in Thermal Coefficients of Expansion in SiC Whisker 6061 Aluminum Composites," *Proceedings of ICCM/5*, Eds., Harringan Jr., W. C., Strife, J., and Dhingra, A., 1985, pp.21-36.

6. Arsenault, R.J. and Shi, N., "Dislocation Generation Due to Differences between the Coefficients of Thermal Expansion," *Materials Science and Engineering*, Vol.81, 1986, pp.175-187.

7. Vogelsang, M., Arsenault, R.J., and Fisher, R.M., "An In-Situ HVEM Study of Dislocation Generation at Al/SiC Interface in Metal Matrix Composites," *Metallurgical Transactions* A, Vol.17A, 1986, pp.379-388.

8. Arsenault, R.J. and Taya, M., "Thermal Residual Stress in Metal Matrix Composite," *Acta Metallurgica*, Vol.35, 1987, pp.650-659.

9. Taya, M. and Mori, T., "Dislocations Punched-Out around a Short Fiber Metal Matrix Composite Subjected to Uniform Temperature Change," Vol.35, No.1, 1987, pp.155-162.

10. Derby, B. and Walker, J.R., "The Role of Enhanced Dislocation Density in Strengthening Metal Matrix Composites," *Scripta Metallurgica*, Vol.22, 1988, pp.529-532.

11. Christman, T., Needleman, A., and Suresh, S., "An Experimental and Numerical Study of Deformation in Metal-Ceramic Composites," *Acta Metallurgica*, Vol.37, No.11, 1989, pp.3029-3050.

12. Llorca, J., Needleman, A., and Suresh, S., "The Bauschinger Effect in Whisker-Reinforced Metal-Matrix Composites," *Scripta Metallurgica*, Vol.24, No.11, 1990, pp.1203-1208.

13. Cook, R.C., Malkua, D.S., and Plesha, M.E., "*Concepts and Applications of Finite Element Analysis*," 3rd Ed., John Wiley & Sons, 1989, pp.163-295.

14. Nair, S.V. and Kim, H.G., "Thermal Residual Stress Effects on Constitutive Response of a Short Fiber or Whisker Reinforced Metal Matrix Composite," *Scripta Metallurgica*, Vol.25, No.10, Oct., 1991, pp.2359-2364.

15. Arsenault, R.J. and Pande, C.S., "Interfaces in Metal Matrix Composites," *Scripta Me-*

tallurgica, Vol.18, 1984, pp.1131-1134.

16. Kim, H.G., "*Micromechanics of Deformation in Short Fiber or Whisker Reinforced Metal Matrix Composites*", Ph.D Dissertation, Department of Mechanical Engineering, University of Massachusetts, Amherst, MA, May, 1992.

17. Takao, Y., Chou, T., and Taya, M., "Effective Longitudinal Young's Modulus of Misoriented Short Fiber Composites," *Journal of Applied Mechanics*, Vol.49, 1982, pp.536-540.

18. Levy, A. and Papazian, J.M., "Elastoplastic Finite Element Analysis of Short Fiber Reinforced Sic/Al Composites: Effects of Thermal Treatments," *Acta Metallurgica*, Vol.39, No.10, 1991, pp.2255-2266.

19. Taya, M. and Arsenault, R.J., "*Metal Matrix Composites, Thermomechanical Behavior*," Pergamon Press, NY, 1989.

20. Nutt, S.R. and Duva, J.M., "A f—Failure Mechanism in Al-Sic Composites," *Scripta Metallurgica*, Vol.20, 1986, pp.1055-1058.

21. Nutt, S.R. and Needleman, A., "Void Nucleation and Fiber Ends in Al-SiC Composites," *Scripta Metallurgica*, Vol.21, 1987, pp.705-710.

22. Murdeshwar, N., "*Fracture Development in a 20 Volume Percent Silicon Carbide Whisker Reinforced Al 2124 Metal Matrix Composites*," Deparrtment of Mechanical Engineering, University of Massachusetts, Amherst, MA, 1989.

23. Needleman, A., "A Continuum Model for Void Nucleation by Inclusion Debonding," ASME *Journal of Applied Mechanics*, Vol.54, 1987, pp.525-531.